PAPER • OPEN ACCESS

Progress in the development of a contactless ultrasonic processing route for alloy grain refinement

View the article online for updates and enhancements.

Progress in the development of a contactless ultrasonic processing route for alloy grain refinement

K A Pericleous[1], C Beckwith[1], V Bojarevics[1], G Djambazov[1], A Dybalska[2], W D Griffiths[2] and C Tonry[1]

[1] Centre for numerical modelling and process analysis, University of Greenwich, UK
[2] Department of metallurgy and materials, University of Birmingham, UK

E-mail: k.pericleous@gre.ac.uk

Abstract. A high frequency tuned electromagnetic (EM) induction coil can be used to induce ultrasonic pressure waves leading to gas cavitation in alloy melts. This is a useful '*contactless*' approach compared to the usual immersed sonotrode technique. One then expects the same benefits obtained in the traditional ultrasonic treatment (UST) of melts, such as degassing, microstructure refinement and dispersion of particles. However, such an approach avoids melt contamination due to probe erosion prevalent in immersed sonotrodes and it has the potential to be used on higher temperature and reactive alloys. Induction stirring due to the Lorentz force produced by the coil is an added benefit, allowing for the treatment of large melt volumes, a current limitation of UST systems. At ultrasonic frequencies (> 20 kHz), due to the 'skin effect' electromagnetic forces vibrate just a thin volume by the surface of the metal facing the induction source. These vibrations are transmitted as acoustic pressure waves into the bulk and to achieve sufficient fluctuation amplitudes for cavitation, acoustic resonance is sought by carefully adjusting the generator frequency. This is akin to the tuning of a musical instrument, where the geometry and sound properties of the metal, crucible and surrounding structure play an important part. In terms of modelling, this is a multi-physics system, since fluid flow with heat transfer and phase change are coupled to electromagnetic and acoustic fields. The various models used and their coupling are explained in this paper, together with the various complications arising by the physics of cavitation. Experimental validation is obtained on a prototype rig featuring a conical induction coil inserted into the melting crucible containing the various alloys being examined. When resonance is reached, measurements demonstrate strong stirring, evidence of cavitation and finally grain refinement.

1. Introduction

Ultrasonic treatment (UST) of alloys at the liquid state, where a vibrating probe oscillating at ~20 kHz immersed in the melt acts as the US source, has been shown to promote grain refinement, dispersing of immersed particles, breaking up of particle clusters, wetting of surfaces and degassing [1-3]. These beneficial effects are attributed to the onset of cavitation of gases present in the liquid, responding to rapid pressure variations induced by an ultrasonic source. Cavitation involves the formation, growth, oscillation, collapse, and implosion of bubbles in liquids [4]. In the vicinity of collapsing bubbles, extreme temperatures (>10000 K [5]) and pressures (>400 MPa [6]) take place. However, despite these positive attributes, the technique has not been widely adopted in industry [3]. There are many reasons for this: the immersed probe tends to erode in the melt causing contamination and consequently the probe (made of expensive materials, e.g. Nb or W) needs to be replaced quite frequently, leading to unnecessary downtime and cost. Furthermore, the cavitation zone appears to be localised in a small volume surrounding the probe, preventing the US treatment of large quantities of metal, or its use in continuous processes. Increase in the sonotrode power does not necessarily improve efficiency, since as it has been shown [7] the concentrated bubble cloud surrounding the probe leads to pressure wave attenuation. Recent efforts to improve volume efficiency in continuous processes rest on increasing the residence time of liquid in the cavitation zone using baffles, e.g. [8] or alternatively, inducing stirring in the melt using either a mechanical stirrer [9], or electromagnetic induction [10].

Due to these limitations, we proposed [11-13] a contactless electromagnetic vibration device that can excite soundwaves in the melt potent enough to cause cavitation. With this concept, shown schematically in figure 1, a high frequency electromagnetic coil is lowered into the melt. Out of phase currents induced in the melt, which is electrically conducting, result in a repulsive force, which prevents contact between the coil and the metal. Several other events take place at the same time, (i) the time-averaged component of the Lorentz force ($\boldsymbol{F}_L = \boldsymbol{J} \times \boldsymbol{B}$) promotes bulk stirring, and (ii) the time dependent (sinusoidal) component of the force vibrates the melt at a frequency selected to cause cavitation. Although at ultrasonic frequencies the force is concentrated in a thin 'skin layer' region, the vibration is transmitted through the bulk through acoustic waves. In order to maximise the pressure wave amplitude at minimum input power, the frequency needs to be tuned to promote acoustic resonance in the treatment vessel [14].
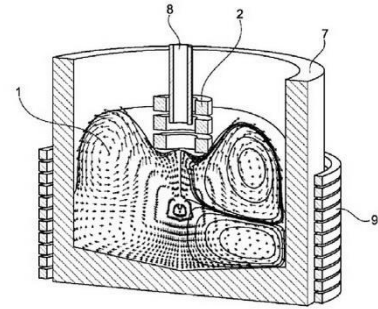

Figure 1. The contactless sonotrode concept [12].

The idea of using electromagnetic vibrations to induce cavitation in liquid metals is not new, but the implementation, that is employing a single induction coil placed in very close proximity to the melt for maximum electromagnetic coupling, plus the use of acoustic resonance to achieve the required wave amplitude is quite novel. In previous studies, Vives [15] coupled AC current running through the melt with an external static magnetic field to promote cavitation. Grants [16] similarly placed an induction heated charge inside the poles of a large DC magnet, to demonstrate cavitation in steel and nano particle dispersion in aluminium for the production of metal matrix composites. Both approaches though demonstrating the principle of contactless EM ultrasonic processing would be difficult to implement in an industrial situation.

In this contribution we demonstrate use of a prototype installation of the contactless sonotrode depicted in figure 1, for grain refinement in aluminium (with or without added grain refiner) and show initial degassing results.

2. Mathematical basis

From the point of view of modelling, this is a truly multi-physics problem, combining magnetically driven flow and heat transfer with acoustics, complicated by the phenomenon of cavitation. Details of the mathematics used have been given in several previous publications and for that reason only a summary will be given here, accompanied by the relevant references.

2.1. MHD flow and heat transfer

The time-dependent conservation equations for mass, momentum and energy are solved, accounting for the effects of electromagnetic interaction and change of phase. An in-house software code 'SPHINX' [17] solves the equations numerically using a spectral colocation technique [18] on a continuously deformable mesh, coincident with the metal volume, as described in [19]. The method enables real-time deformation of the liquid free surface based on the instantaneous balance of forces acting on it. A description of the main equations follows:

Momentum and Continuity

$$\partial_t \mathbf{v} + (\mathbf{v} \cdot \nabla)\mathbf{v} = -\rho^{-1}\nabla p + \nabla \cdot (\nu_e(\nabla \mathbf{v} + \nabla \mathbf{v}^T)) + \rho^{-1}\mathbf{f}_m + S_D \tag{1}$$

$$\nabla . \mathbf{v} = 0 \tag{2}$$

where $\mathbf{v}$ is the velocity, ρ the density, p the pressure, ν_e the effective viscosity (sum of laminar and turbulent contributions), $\mathbf{f}_m$ the volumetric electromagnetic (Lorentz) force and S_D is a Darcy flow resistance term that accounts for the macroscopic effect of phase change on flow in mushy zones. The boundary conditions assume no-slip at solid walls ($\mathbf{v}$=0) or alternatively free surface dynamic and kinematic conditions when the liquid metal is detached from any solid surface.

Energy conservation

$$\frac{\partial(\rho C_p T)}{\partial t} + \nabla(\rho C_p T\mathbf{v}) = \nabla(k_{eff}\nabla(T)) + q_e + q_L \tag{3}$$

where T is the temperature, C_p the specific heat and k_{eff} the effective conductivity. The last two terms in equation (3) represent Joule heating, q_e and latent heat release, q_L

$$q_e = \frac{J^2}{\sigma} \; ; q_L = -\frac{\partial}{\partial t}(\rho f_L L) - \nabla.(\rho\mathbf{v}f_L L) \tag{4}$$

where σ is the electrical conductivity of the liquid and L the latent heat constant.

The liquid fraction f_L is defined as a function of temperature T:

$$f_L = \begin{cases} 1 & T > T_L & \text{liquid} \\ \left(\frac{T-T_s}{T_L-T_s}\right) & T_s \leq T \leq T_L & \text{mushy zone} \\ 0 & T < T_s & \text{solid} \end{cases} \tag{5}$$

Then

$$S_D = \frac{\mu}{K}\boldsymbol{v} \; ; \; K = \frac{f_L^3}{\zeta(1-f_L)^2} \tag{6}$$

Heat transfer boundary conditions are stated for free-surface radiation and wall loss, described in [17, 19]. The effective heat transfer at solid walls is then given by

$$-\rho C_p \, \alpha_e \partial_n T = h(T - T_w) \tag{7}$$

where *h(T)* is the heat transfer coefficient, with free surface radiation given by:

$$-\rho C_p \, \alpha_e \partial_n T = \varepsilon\sigma_R(T^4 - T_w^{\;4}) \tag{8}$$

with α_e being the turbulent thermal diffusion coefficient. Turbulence is modeled using the *k-ω* model of Wilcox [20].
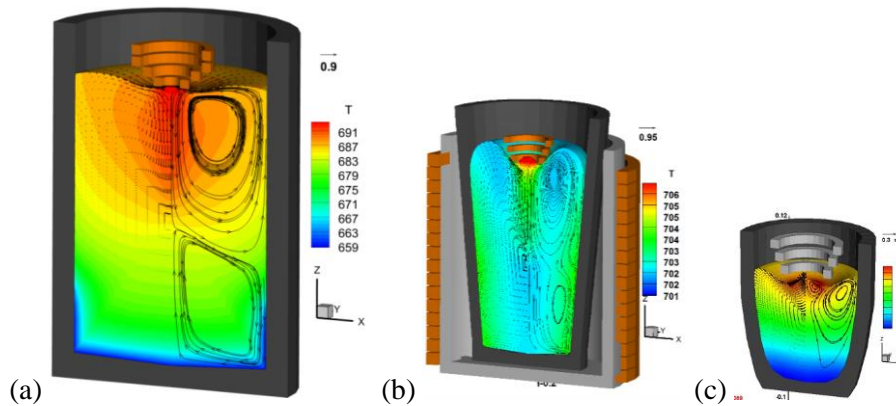

Figure 2. Computed surface deformation, flow patterns and temperature in three crucibles of varying size containing aluminium: (a) 50 kg, (b) 10.5 kg, (c) 5 kg. Note, (a) and (b) include the influence of the furnace coil as well as the top coil. Crucibles (b) and (c) were used in experiments, with (c) used for particle tracking (PEPT) studies.

Typical simulations are shown in figure 2, demonstrating the application of the top coil sonotrode in three different vessel sizes. Ceramic crucibles (b) and (c) correspond to experimental configurations, while the large crucible (a) is a hypothetical application to highlight the scaleup potential of the process.

As the top coil (typically 1700 A at 10 kHz) moves towards the metal free surface, the surface deforms by repulsion. At the same time strong stirring is observed due to combined induction from the furnace and top coils in crucibles 2(a) and 2(b)). In crucible 2(c) the top coil acts alone, but still a deep toroidal vortex is observed due to the time-averaged Lorentz force. In addition to stirring considerable Joule heating is generated by the coil, leading to a hot spot near the surface coinciding with the coil axis. In the same position the free surface is elevated as the Lorentz force decays to zero.

2.2. Magnetic induction as a source of sound

The AC magnetic field of angular frequency ω due to the coil, B, and the induced current, J, can be expressed into real and imaginary components (subscripts $_R$ and $_I$ respectively). The Lorentz force can then be split into time-averaged and time-dependent components:

$$
\boldsymbol{F} = \boldsymbol{J} \times \boldsymbol{B} = \bar{F} + \tilde{F} \quad \text{then,}
$$
$$
\bar{F} = \frac{1}{2}(J_R B_R + J_I B_I) = \frac{1}{2\mu\delta} B_o^2 e^{-2\frac{x}{\delta}}, \qquad \tilde{F} = \frac{1}{2\mu\delta} B_o^2 e^{-2\frac{x}{\delta}} \sqrt{2}\cos\left(2\omega t - 2\frac{x}{\delta} + \frac{\pi}{4}\right) \tag{9}
$$

where $\delta = \sqrt{\frac{2}{\mu\omega\sigma}}$ is the skin depth indicating the force penetration into the fluid.

The mean value $\bar{F}$, is then responsible for bulk stirring as shown in figure 2, while the sinusoidal part $\tilde{F}$ is the source of vibration. It is important to note (a) that the vibration frequency is double that of the supply current, (b) that the force decays within the skin-depth distance δ from the liquid free surface, hence the importance of acoustic resonance in achieving the required pressure amplitude for cavitation in the bulk volume (see equation (11) below).

2.3. Sound wave propagation

The time-dependent force component $\tilde{F}$, is the source of sound waves, computed in the time domain by solving the Euler form of the momentum equations, generating a perturbation velocity field $\tilde{v}$:

$$
\frac{\partial p}{\partial t} + \rho c^2 \frac{\partial \tilde{v}}{\partial x} = S; \ \rho \frac{\partial \tilde{v}}{\partial t} + \frac{\partial p}{\partial x} = \tilde{F} \tag{10}
$$

A staggered scheme (in space and time) is used to solve equations (10), with details given in Djambazov *et al.* [21]. The source S represents pressure contributions due to cavitating bubbles [22]. The solution domain for sound extends beyond the melt to include the crucible and surrounding structures accounting for transmission and reflection of sound through the crucible walls. Constant pressure is assumed at the liquid free surface and a sound-hard boundary (zero flux) is applied at the coil surface. Details of the approach are given in [14].

A characteristic of this process is the appearance of pressure nodes/antinodes deep inside the melt volume during resonance, marking likely cavitation regions (e.g. see figure 3). This contrasts with the immersed sonotrode case, where cavitation activity is restricted to an area surrounding the vibrating probe, leading to shielding effects due to bubble concentration that limit process efficiency.

2.4. Cavitation

Cavitation of dissolved gases is considered essential in encouraging nucleation, hence leading to grain refinement in alloys. Seeking the resonant frequencies of the system, ensures pressures greater than the Blake threshold where cavitation may occur can be obtained. The Blake threshold is calculated from

$$
P_B = p_0 \left(1 + \sqrt{\frac{4}{27} \frac{\xi^3}{1+\xi}} \right), \xi = \frac{2\sigma}{R_0 p_0}, \tag{11}
$$

where p_0 is the ambient pressure, σ the interfacial tension and R_0 the bubble radius. For example, bubbles with a radius $R_0 = 5 \times 10^{-6}$ m, an interfacial tension for aluminium and air of $\sigma = 1.1$ N/m and with $p_0 = 101325.0$ Pa gives a Blake threshold of 254 kPa.
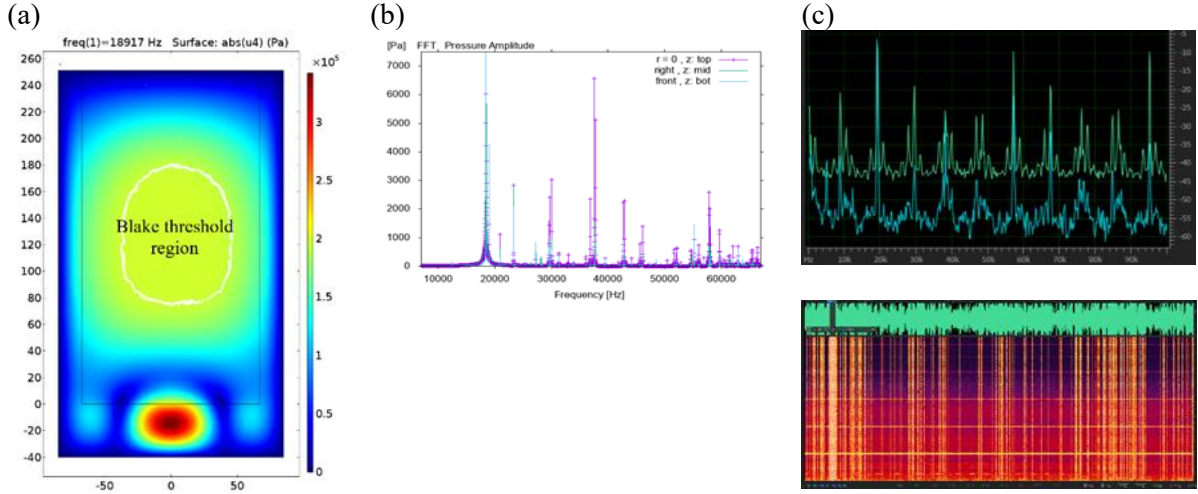
Figure 3. (a) Computed sound-field in a cylindrical crucible with the top coil acting as the sound source (f = 18917 Hz). (b) Predicted sound spectrum obtained with a driving frequency f=18917 Hz, showing several excited harmonics. (c) Experimental sound spectrogram showing intermittent cavitation noise; the accompanying spectrum compares loud and silent regions.

Bubble dynamics due to the pressure change are handled using the Keller-Miksis equation [23]

$$\left(1 - \frac{\dot{R}}{c}\right) R\ddot{R} + \frac{3}{2}\dot{R}^2\left(1 - \frac{\dot{R}}{3c}\right) = \frac{1}{\rho_l}\left(1 + \frac{\dot{R}}{c} + \frac{R}{c}\frac{d}{dt}\right)[p_l - p(t)], \tag{12}$$

which accounts for liquid compressibility and damping. Then p_l represents the liquid pressure at the liquid gas interface defined by

$$p_l = p_g - \frac{2\sigma}{R} - \frac{4\mu\dot{R}}{R}, \tag{13}$$

where σ is the surface tension, μ is the liquid viscosity, and p_g is the pressure in the gas at the interface, calculated from

$$\frac{\partial p_g}{\partial t} = \frac{3}{R}\left[(\gamma - 1)\left(k_T \left.\frac{dT}{dR}\right|_{r=R}\right)\gamma p_g\dot{R}\right] \tag{14}$$

γ being the polytropic index, and k_T the thermal conductivity of the gas. The temperature gradient at the bubble surface is calculated using

$$\left.\frac{dT}{dR}\right|_{r=R} = \frac{T - T_\infty}{\sqrt{RD}/3(\gamma - 1)\dot{R}} \tag{15}$$

where D is the gas diffusivity, and T_∞ the bulk temperature of the liquid. The Keller-Miksis equation accounts for acoustic radiation terms that address the lack of damping in the original Rayleigh-Plesset equation that overpredicts bubble oscillation amplitudes post collapse. A variable-step variable-order Adams-Bashforth-Moulton method was chosen to solve the Keller-Miksis equation.

To account for the change in void fraction β during a period of pressure oscillation on sound transmission the Caflisch model was used [24]. Based on Trujillo [25] a time harmonic solution of the Caflisch model, introduces dissipation functions $\mathcal{A}$ and $\mathcal{B}$ based on the void fraction $\beta = \frac{4}{3}\pi R^3 N$:

$$\mathcal{A} = -\frac{\rho_l\omega^2}{\pi}\int_0^{2\pi}\frac{\partial\beta}{\partial\tau}\sin\tau\,d\tau, \mathcal{B} = -\frac{\rho_l\omega^2}{\pi}\int_0^{2\pi}\frac{\partial\beta}{\partial\tau}\cos\tau\,d\tau, \tag{16}$$

where N is the assumed number of bubbles. These relations can be used in a Helmholtz equation of the form:

$$(\nabla^2 + k^2)p = 0 \tag{17}$$

where k is a modified wave number and p the pressure:

$$k^2 = \left(\frac{\omega}{c}\right)^2 - \frac{\mathcal{A}(p)}{|p|} - i\frac{\mathcal{B}(p)}{|p|} \tag{18}$$

3. Experimental results

The general experimental setup is shown in figure 4. An induction furnace was used to melt and sonicate aluminium in ceramic crucibles. Both cylindrical and tapered crucibles were used with charges ranging from 8 -10 kg. The top coil was lowered into the crucible once the charge was fully melted and then the main furnace coil was switched off to maintain the temperature at around 700 °C.

3.1. Cavitation detection

An ultrasonic microphone was used to detect noise emitted from the crucible and the frequency adjusted until the recorded signal revealed the presence of broad-spectrum noise as a sign of cavitation. Figure 3(c) shows a typical spectrogram, plotting frequency against time. The continuous horizontal lines correspond to the top coil driving frequency, its harmonics and subharmonics. The vertical lines indicate cavitation activity, which is always intermittent. We think this is because the presence of bubbles during cavitation alters the speed of sound locally interrupting resonance. As the pressure amplitude diminishes, cavitation stops, resonance returns, and the cycle repeats. As depicted in figure 3(c) (top) comparing quiet and loud regions in the spectrogram, the spectrum retains its harmonics, but the sound level diminishes by ~ 20 dB.

3.2. Grain refinement

Alloy grain refinement experiments were conducted in a cylindrical clay-graphite crucible with internal and external diameters of 135 and 170 mm respectively, and depth 280 mm. For each experiment the crucible was filled with about 8.5 kg metal, either commercial purity aluminium (CP-Al), or CP-Al with the addition of 0.2 wt.% Al–5Ti–1B grain refiner (100 ppm Ti, 20 ppm B). Figure 4 shows the top coil positioned centrally above the liquid metal surface and above it the Ultramic®200K digital ultrasonic microphone for recording the ambient ultrasonic noise emitted around the crucible during processing. Recorded sound was observed in the form of a FFT (Fast Fourier Transform) sound spectrum in real-time.

Figure 4.
Experimental setup.

Conditions generating resonance accompanied by cavitation noise, (coil frequency and melt temperature), were maintained for about 5 minutes to produce samples for grain structure analysis. The samples were taken using the KBI ring test [25], where liquid metal is poured into a steel ring with an outside diameter of 75 mm, inside diameter 50 mm and height 25 mm, placed on an insulating silica brick and left to solidify. For grain size characterization, the base of the cylindrical samples was removed to about 3 mm above their base and ground (see figure 5), polished and etched with either Poulton's or Keller's solution and the average grain size determined using the mean linear intercept method.

Figures 6 and 7 show the recorded spectrograms and post mortem grain structures of samples obtained following ultrasound treatment. Figure 6 shows the grain of CP-Al at 700°C pre-and post-treatment with 1700 A, 9.35 kHz current through the coil. Control of melt temperature during ultrasound processing found to be important. It must be kept low enough to promote cavitation with this method. In experiments it was maintained at 40 °C above the
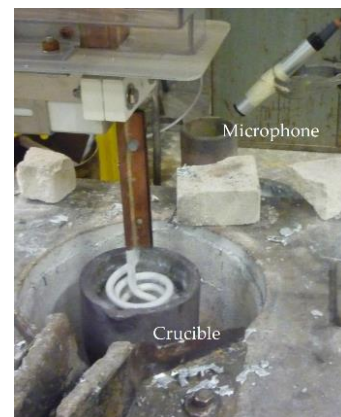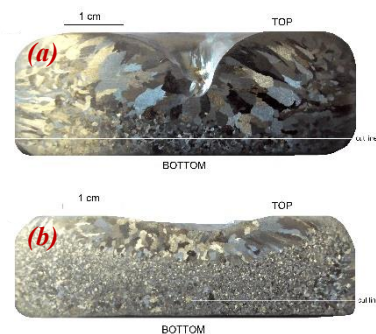

Figure 5. Sectioned KBI ring test samples (a) unprocessed, (b) processed.

melting point, which for pure Al was 700 °C, the minimum value for pouring the liquid metal in a casting. For this CP-Al experiment (figure 6), the grain size reduction was about 63%, (a reduction from 256 ± 12 to 95 ± 1 μm). Cavitation is believed to induce heterogeneous nucleation by (i) forced wetting of non-wetted particles present in the melt, resulting in an increased number of nucleation sites, (ii) local undercooling due to pressure changes when bubbles collapse or (iii) undercooling of the melt at the bubble surface when the bubble rapidly expands. In the case of CP-Al, the number of non-wetted particles would be smaller than in alloys with grain refiner addition, making grain refinement more difficult.

The addition of grain refiner (0.2% Al–5Ti–1B) increases the number of active nuclei so that all three mechanisms of cavitation-induced heterogeneous nucleation can take place. Figure 7 shows the grain size reduction achieved for CP-Al with a grain refiner processed for 5 mins at 9.41 kHz. A grain sizes reduction from 223 ± 5 to 121 ± 2 μm was obtained.
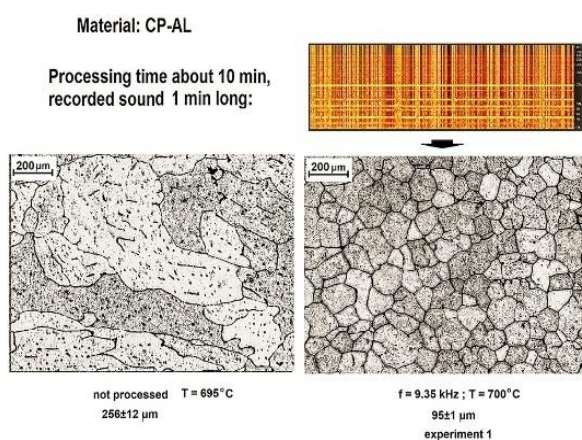

Figure 6. Commercial purity aluminium (CP-Al) showing grain structures before and after processing. Grain size is reduced from 256 μm to 95 μm.
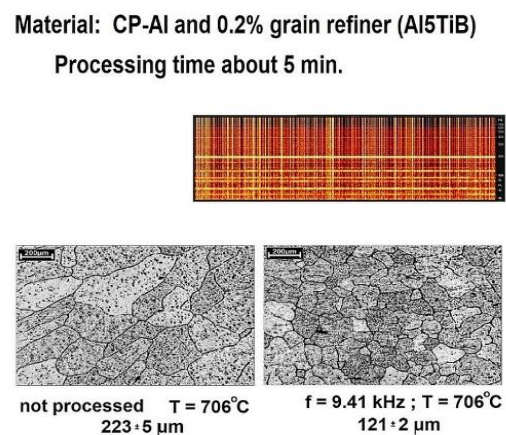
Figure 7. Commercial purity aluminium (CP-Al) showing grain structures before and after processing. Grain size is reduced from 223 μm to 121 μm.

3.3. Correlation between grain refinement and sound frequency spectrum
The basic concept behind the contactless sonotrode relies on the initiation of gas cavitation activity using acoustic resonance as the main driver for grain refinement. Numerical simulations provide an indication of the likely resonant modes, given the sound properties and geometry of the alloy and crucible materials [14]. However, since these properties can vary unpredictably (especially so in ceramic crucibles), the experiment traverses the space about the indicated central frequency value using the spectrogram as an indicator of the most potent value, judged by the frequency of broadband noise bursts. Also evident in all spectrograms is that the cavitation activity as shown by the vertical lines is intermittent. This may be due to local changes in sound velocity in the melt as clouds of bubbles appear and disappear, which would disrupt the resonant conditions.

4. Concluding remarks
This paper shows a contactless electromagnetic processing technique that can generate ultrasonic waves in liquid metals in a crucible, strong enough to produce cavitation. This technique was tested experimentally to treat aluminium alloys in the liquid state with and without commercial grain refiners, achieving substantial grain reduction in both cases. The computational model couples fluid flow, heat transfer, electromagnetics and soundwave generation. Validation was carried out against experimental observations in aspects that are important for the process. These confirm the predicted free surface

depression by the coil, induction driven flow leading to strong mixing and the presence of cavitation during resonant conditions. Acoustic resonance was found to be necessary for pressure waves strong enough for cavitation. This means in practice that geometrical details and material sound properties of the setup become important for successful implementation. Using this technique, it has been possible to produce grain-refined samples of both pure aluminium and aluminium with grain refiner added. Future work aims to test the technique in high temperature and reactive alloys, where the traditional immersed sonotrode method cannot be used.

References
[1]   Abramov O V 1987 *Ultrasonics* **25** 73
[2]   Campbell J Effects of vibration during solidification 1981 *Int Metals Reviews* **26** 71
[3]   Eskin G I and Eskin D G 2015 *Ultrasonic treatment of light alloy melts* Taylor & Francis, CRC Press
[4]   Leighton T G 1994 *The Acoustic Bubble* (London: Acad. Press)
[5]   Flannigan D J and Suslick K S 2005 *Nature* **434** 52–5
[6]   Tzanakis I, Eskin D G, Georgoulas A and Fytanidis D 2014 *Ultson* **21** 866–78.
[7]   Lebon G S B, Tzanakis I, Pericleous K A and Eskin D 2017 *Ultson* **42** 411-21
[8]   Lebon G S B, Pericleous K A, Tzanakis I and Eskin D 2016 *Int. J. Cast Metals Res.* **29** 324
[9]   Dieringa H, Katsarou L, Buzolin R, Szakacs G, Horstmann M, Wolff M, Mendis C, Vorozhtsov S and StJon D 2017 *Metals* **7(10)** 388
[10]   Xuan Y, Dong A and Nastac L 2019 In: *Light Metals*. Eds Chesonis C *et al.* (Cham: Springer)
[11]   Bojarevics V, Djambazov G and Pericleous K A 2015 *Metall. Mater. Trans. A* **46** 2884-92
[12]   Jarvis D J, Pericleous K A, Bojarevics V and Lehnert C 2019 *'VibroEM'* Patent US 10, 207, 321 B2
[13]   Pericleous K A, Bojarevics V, Djambazov G, Dybalska A, Griffiths W D and Tonry C 2019 *Shape Casting: 7th Int. Symp. Celebr. Prof. John Campbell's 80th Birthday*, eds Tiryakioğlu M *et al.* (Cham; Springer) 239-52
[14]   Tonry C E H, Djambazov G S, Dybalska A, Bojarevics V, Griffiths W D and Pericleous K A 2019 *Light Metals* TMS Series (Cham: Springer)
[15]   Vives C 1996 *J. Crystal Growth* **158** 118
[16]   Grants I, Gerbeth G and Bojarevics A 2015 *J. Appl. Phys.* **117** 204
[17]   Pericleous K A and Bojarevics V 2007 *Progress in Comp. Fluid Dynamics* **7** Nos. 2/3/4
[18]   Canuto C, Hussaini M Y, Quarteroni A, and Zang T A 2006 *Spectral methods. Fundamentals in single domains* (Berlin: Springer-Verlag)
[19]   Bojarevics V, Harding RA, Pericleous KA and Wickins M 2004 *Metall. Mat. Trans. B*, **35** 785-803
[20]   Wilcox D C 1998 *Turbulence Modelling for CFD*, 2nd ed., (California: DCW Industries)
[21]   Djambazov G S, Lai C H and Pericleous K A 2000 *AIAA J.* **38** 16–21
[22]   Lebon G S B, Tzanakis I, Djambazov G, Pericleous K A and Eskin, D G 2017 *Ultson* **37** 660–8
[23]   Keller J B and Miksis M 1980 *J. Acoust. Soc. Am.* **68** 628–33
[24]   Caflish R E, Miksis M J, Papanicolaou G C and Ting L 1985 *J. Fluid Mech.* **153** 259–73
[25]   Trujillo F J 2018 *Ultson* **47** 75-98
[26]   Murty B S, Kori S A and Chakraborty M 2002 *Int. Mater. Rev.* **47** 3–29